J. Fluid Mech. (1995), *vol.* 285, *pp.* 181–202

Direct computation of the sound from a compressible co-rotating vortex pair

By BRIAN E. MITCHELL, SANJIVA K. LELE† AND PARVIZ MOIN‡

Department of Mechanical Engineering, Stanford University, Stanford, CA 94305, USA

(Received 15 May 1993 and in revised form 17 September 1994)

The far-field sound generated by compressible co-rotating vortices is computed by direct computation of the unsteady compressible Navier–Stokes equations on a computational domain that extends to two acoustic wavelengths in all directions. The vortices undergo a period of co-rotation followed by a sudden merger. The directly computed far-field sound is compared to the prediction of the acoustic analogy due to Möhring (1978, 1979), a modified form of the analogy developed by Lighthill (1952), and an acoustic analogy derived by Powell (1964). All three predictions are in excellent agreement with the simulation. Results of far-field pressure fluctuations from an acoustically non-compact, co-rotating vortex pair are also presented. In this case, the vortex sound theory over-predicts the sound by 65% in accordance with the analysis of Yates (1978).

1. Introduction

As a step towards direct computation of aerodynamic sound generation in free shear flows, the far-field sound from co-rotating vortices is computed directly by solving the compressible Navier–Stokes equations. The difficulties encountered in the direct computation of aeroacoustic fields have been discussed in a review paper by Crighton (1988). These difficulties include the large extent of the acoustic field as compared to the flow field, the small energy of the acoustic field, the possibility that numerical discretization may serve as a significant source of sound, and errors arising due to inaccurate boundary conditions.

Direct computations of the unsteady compressible Navier–Stokes equations for a domain that includes both the near and far field offer the advantage that near-field quantities, i.e. the source terms in an acoustic analogy, can be directly measured along with the far-field sound. This allows a direct check of acoustic theory which is desirable since not all of the assumptions invoked in the derivation of acoustic theory are satisfied in complex flows. For example, acoustic analogies separate the 'sources' from the propagation effects; this distinction is rigorous only for low-Mach-number flows (Crow 1970). Also, it is often necessary to use a simplified expression for the source terms. Furthermore, the source terms in many acoustic analogies are based on the incompressible part of the near field (Crow 1970). Since computational and experimental data cannot be decomposed into compressible and incompressible parts, an additional approximation is introduced when the full compressible data are used to evaluate the source terms.

In addition to allowing a quantitative check of acoustic theory, knowledge of both

† Also with Department of Aeronautics and Astronautics, Stanford University.
‡ Also with NASA-Ames Research Center.

near- and far-field quantities will facilitate the identification of coherent structures and other flow features responsible for sound generation in more complex flows. Hopefully, such knowledge will lead to effective strategies for modelling the noise generation and its control.

The goals of this study are several. First, the basic process of sound generation is investigated in a simple unsteady flow. Secondly, the quantitative validity of existing acoustic analogies due to Lighthill (1952), Powell (1964), Howe (1975), and Möhring (1978, 1979) are tested. Investigating the ability of acoustic theory to predict the sound generated by co-rotating vortices is a necessary step towards understanding the applicability of acoustic theory in predicting the sound generated by more complex vortical flows such as mixing layers and jets where acoustic terms are specified using data from direct numerical simulations of either the incompressible or compressible Navier–Stokes equations. Thirdly, extensions of existing theories are pursued. Lastly, we seek to gain insight and develop computational techniques to facilitate future studies of sound generation in more complex flows.

The sound from co-rotating vortices was chosen as a logical extension of the work of Colonius, Lele & Moin (1991, 1994) who computed the scattering of sound waves by a single compressible vortex. Co-rotating vortices, in contrast to the scattering of sound waves by a single vortex, generate sound due to the inherent unsteadiness of the flow field. The generated sound is predicted to be that of a rotating quadrupole (Powell 1964; Müller & Obermeier 1967; Lyamshev & Skvortsov 1988; Yates 1978).

In §2, we present a brief summary of relevant acoustic theory and specialize the results to point vortices. Section 3 introduces the flow and reviews the computational method, and in §4 the results of the simulations are presented and compared to predictions of aeroacoustic theory. A summary of conclusions is presented in §5.

2. Aeroacoustic theory

Several aeroacoustic analogies have been proposed in the literature for predicting the far-field sound radiated by unsteady flows. Expressions for the far-field acoustic pressure given by application of existing theories to two-dimensional, acoustically compact, vortical flows are summarized in §2.1. These will be used in §4 to predict the sound generated by the co-rotating vortices. We observe that the vortex sound theory of Möhring (1978, 1979) is the simplest approach for predicting the sound from two- and three-dimensional, acoustically compact, compact vortical flows. This theory provides the leading-order quadrupole prediction of the far-field sound.

A variety of assumptions are frequently invoked in aeroacoustic theory including compact flow, compact source, and low Mach number. The compact flow assumption requires that the vorticity is always zero outside a fixed finite region around the origin. The compact source assumption requires that the source region is acoustically compact. The low-Mach-number assumption requires that the near field is sufficiently incompressible. These assumptions will be invoked in some of the discussion that follows.

2.1. *Existing aeroacoustic theory*

The first acoustic analogy was due to Lighthill (1952) who rearranged the exact continuity and momentum equations into a wave equation with a source term on the right-hand side

$$\left(\frac{\partial^2}{\partial t^2} - c_0^2 \nabla^2\right) \rho' = \frac{\partial^2 T_{ij}}{\partial x_i \partial x_j}, \tag{1}$$

where

$$T_{ij} = \rho u_i u_j + (P - c_0^2 \rho)\, \delta_{ij} + \text{viscous terms}$$

and where P is the pressure, ρ is the density, u_i is the velocity in the ith direction, and c_0 is the ambient speed of sound. The prime denotes a fluctuating quantity, i.e. $\rho = \rho_0 + \rho'$. Typically, the source term is approximated by $T_{ij} = \rho_0 u_i u_j$ (Crow 1970; Obermeier 1985). Lighthill's equation explicitly shows the quadrupole nature of the acoustic sources. The solution of (1) for an acoustically compact source and compact flow in two dimensions is

$$P'(\boldsymbol{x}, t) = \frac{1}{2\pi}\left(\frac{x_i x_j}{r^2}\right)\int_0^\infty \frac{\partial^2}{\partial t^{*2}}\left(\int T_{ij}(\boldsymbol{y}, t^*)\,\mathrm{d}\boldsymbol{y}\right)\mathrm{d}\xi, \tag{2}$$

where $t^* = t - r/c_0\cosh(\xi)$ and $r^2 = x_k x_k$. The derivation of (2) is given in Appendix A. Lighthill develops a three-dimensional solution and Ffowcs Williams & Hawkings (1968) derive a two-dimensional solution that is different, but equivalent to (2).

Unfortunately, the area integral of T_{ij} is divergent for a compact flow with non-zero circulation, invalidating the use of (2) as a solution of (1). However, since the far-field acoustic pressure depends on the second time derivative of the area integral of T_{ij}, (2) can still be used for compact flows with finite circulation. This is achieved by separating the steady component related to the net circulation from the more rapidly decaying unsteady part; the latter produces a net contribution to (2). The details of this procedure are explained in §4. The solution of (1) presented by Ffowcs Williams & Hawkings (1968) also suffers from divergence of integrals.

Although the decay rate of the velocity is sufficiently rapid in three dimensions to ensure the convergence of the integral of T_{ij}, the algebraic decay rate still makes it difficult to know *a priori* where the integral can be truncated (Crow 1970). Such a truncation is necessary in a practical application of the theory. This difficulty is avoided in the acoustic analogy first introduced by Powell (1964) and later by Howe (1975):

$$\left(\frac{1}{c_0^2}\frac{\partial^2}{\partial t^2} - \nabla^2\right)P' = \boldsymbol{\nabla}\cdot(\rho\boldsymbol{\omega}\times\boldsymbol{u}), \tag{3}$$

where $\boldsymbol{\omega} = \boldsymbol{\nabla}\times\boldsymbol{u}$. This form yields a well-defined source region, i.e. the region of non-zero vorticity. Two assumptions have been made in deriving (3): that the flow is inviscid; and that the terms

$$\frac{\partial^2}{\partial t^2}\left(\frac{1}{c_0^2}P - \rho\right) + \boldsymbol{\nabla}\cdot\left(\boldsymbol{\nabla}\tfrac{1}{2}\rho u_i u_i - \boldsymbol{u}\frac{\partial\rho}{\partial t} - \tfrac{1}{2}u_i u_i \boldsymbol{\nabla}\rho\right)$$

which should be included in the source term on the right-hand side can be neglected. This is an excellent assumption for low-Mach-number moderate-Strouhal-number high-Reynolds-number flows; see Powell (1964) and Howe (1975). The first two neglected terms contribute to the viscous monopole discussed by Kambe (1984) and Obermeier (1985). In §4, we verify that the viscous monopole is negligible for co-rotating vortices.

Note that (3) expresses the acoustic sources as a distribution of dipoles over the source volume and, since quadrupole sound is expected, there must be dipole cancellations in the integrals involved with its solution. Because of these cancellations, retarded time differences cannot be ignored (as was done between (A 4) and (A 5) in the derivation of (2)) and the resulting convolution integrals are expensive to evaluate numerically.

There are two approaches to deal with this difficulty. The first is to solve (3) by the numerical solution of the wave equation. However, Crighton (1988) has cautioned that numerical errors may spoil the required dipole cancellations, leading to an erroneous

over-prediction of the far-field sound. Our results, presented in §4, do not suffer from this problem. Equation (3) can also be solved using a multipole expansion to determine the quadrupole component explicitly. This approach is the basis of Appendix C where it is shown that a multipole expansion of Powell's equation can be used to derive Möhring's equation. Powell (1964) also performs a multipole expansion; however, his quadrupole term involves a product of velocity and vorticity, whereas the results of Appendix C only involve the vorticity. Since, (3) is being solved numerically, no assumptions about acoustical compactness are made.

Möhring (1978, 1979) avoids the problems of Lighthill (1952) and Powell (1964) by predicting quadrupole sound from a source region of non-zero vorticity. Möhring's three-dimensional result (Möhring 1978) is

$$P'(\boldsymbol{x}, t) = \frac{\rho_0}{12\pi c_0^2} \frac{x_i x_j}{r^3} \dddot{Q}_{ij}(t - |\boldsymbol{x}|/c_0), \tag{4}$$

where Q_{ij} is given by the second-order moments of vorticity

$$Q_{ij}(t) = \int (\boldsymbol{y} \times \boldsymbol{\omega}(\boldsymbol{y}, t))_i \, y_j \, \mathrm{d}\boldsymbol{y}. \tag{5}$$

Equation (4) assumes low Mach number, a compact flow, and a compact source. Möhring's two-dimensional result (Möhring 1979) is derived in Appendix B using the method of matched asymptotic expansions following the derivation of Möhring's three-dimensional result by Kambe, Minota & Takaoka (1993). The far field pressure fluctuations are predicted to be

$$P'(\boldsymbol{x}, t) = \frac{\rho_0}{8\pi c_0^2} \int_0^\infty [\dddot{Q}_1(t^*) \cos(2\theta) + \dddot{Q}_2(t^*) \sin(2\theta)] \, \mathrm{d}\xi, \tag{6}$$

where $t^* = t - (r/c_0)\cosh(\xi)$, θ is measured with respect to the x-axis, and where the source terms, Q_1 and Q_2, are the second-order moments of vorticity

$$Q_1 \equiv 2 \int\int xy\omega \, \mathrm{d}x \, \mathrm{d}y, \quad Q_2 \equiv \int\int (y^2 - x^2) \, \omega \, \mathrm{d}x \, \mathrm{d}y. \tag{7}$$

Kambe *et al.* (1993) have proposed extending Möhring's three-dimensional result to include higher-order multipoles and have demonstrated that the octupole term is important in the oblique collision of vortex rings. The form of the extension for the two-dimensional Möhring equation is presented in Appendix B. We observed that these higher-order multipoles are negligible for the co-rotating vortices.

It is interesting to note that (4) cannot be directly converted to (6) in the usual way, see for example Lamb (1932, §302), by integration along the z-axis because assumptions of vorticity localization would be violated. In fact, such a direct conversion would under-predict the pressure levels by a factor of 2/3. A unified representation that includes Möhring's two- and three-dimensional expressions is given in Appendix C.

2.2. *Co-rotating point vortices*

Although the sound from co-rotating viscous compressible vortices cannot be determined analytically, the simplified case of inviscid point vortices does yield analytical solutions. The key feature of point vortices is the periodicity of the flow, i.e. the vortices rotate around one another with period $8\pi^2 R^2/\Gamma_0$ where R is the half-separation distance and Γ_0 is the circulation of each vortex (see figure 1; U_0 and r_0 will be defined in §3). Our approach will be to use the known results for the near field of point vortices to prescribe the source region of Möhring's equation (6).

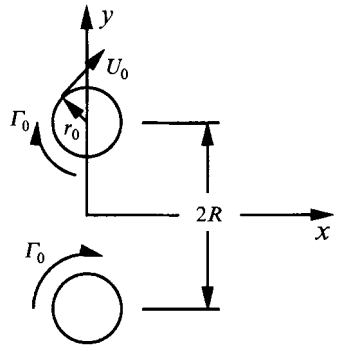

FIGURE 1. Schematic diagram of flow configuration.

The time-harmonic form of Möhring's equation given in Appendix B (equation (B 8)) can be expressed as

$$P'(r,\theta,t) = \frac{\rho_0 \Omega^3}{16 c_0^2} \mathrm{H}_2^{(1)}\left(\frac{\Omega r}{c_0}\right)[\hat{Q}_1(\Omega)\cos(2\theta) + \hat{Q}_2(\Omega)\sin(2\theta)]\,\mathrm{e}^{-\mathrm{i}\Omega t}, \tag{8}$$

where $\hat{Q}_1$ and $\hat{Q}_2$ are the Fourier transforms of Q_1 and Q_2 defined in (7). Equation (8) corrects an erroneous result developed by Lyamshev & Skvortsov (1988) using a different method.

In the flow considered in this paper, the vortices are initially aligned along the y-axis and rotate clockwise around one another,

$$Q_1 = -2\Gamma_0 R^2 \sin(2\Omega_0 t), \quad Q_2 = -2\Gamma_0 R^2 \cos(2\Omega_0 t), \tag{9}$$

where $\Omega_0 = \Gamma_0/(4\pi R^2)$ corresponds to the rotation rate of the vortices around one another. The appearance of $2\Omega_0$ is due to the symmetry of the problem. Use of (8) and (9) then leads to a theoretical prediction for the sound from point vortices:

$$P'(r,\theta,t) = \frac{-\rho_0 \Gamma_0^4}{64\pi^3 R^4 c_0^2}\left(\mathrm{J}_2\left(\frac{2\Omega_0 r}{c_0}\right)\sin(2\theta + 2\Omega_0 t) + \mathrm{Y}_2\left(\frac{2\Omega_0 r}{c_0}\right)\cos(2\theta + 2\Omega_0 t)\right), \tag{10}$$

where $\mathrm{J}_2(z)$ and $\mathrm{Y}_2(z)$ are the second-order Bessel functions of the first and second kind respectively. A characteristic solution for point vortices is shown in figure 2. The double spiral pattern clearly illustrates the rotating quadrupole nature of the sound. Note also that the sound waves are cylindrical in the far field.

Co-rotating point vortices have also been considered by Powell (1964), Müller & Obermeier (1967), and Yates (1978). Müller & Obermeier (1967) derived a quadrupole expression for the far-field sound that is equivalent to (10). Yates (1978) considered the sound generated by acoustically non-compact co-rotating point vortices and developed a series solution containing quadrupoles, octupoles, and higher-order multipoles. Yates found that the coefficient of the quadrupole term is a strong function of the co-rotation Mach number, $M_r = U_r/c_0$, where the co-rotation velocity, U_r is $U_r = \Omega R$. On the basis of his results, Yates concluded that the co-rotating vortices are acoustically compact for $M_r < 0.1$. As discussed by Yates, this is a somewhat surprising result since the ratio of the acoustic wavelength to R is 31 for $M_r = 0.1$. In the compact limit, Yates' results are identical to (10).

Equation (10) predicts that the pressure intensity, $\overline{P^2}$, scales as U^7 in the acoustic far field. This differs from the three-dimensional result first reported by Lighthill (1952) who showed that the pressure intensity scaled as U^8, but it is in agreement with other

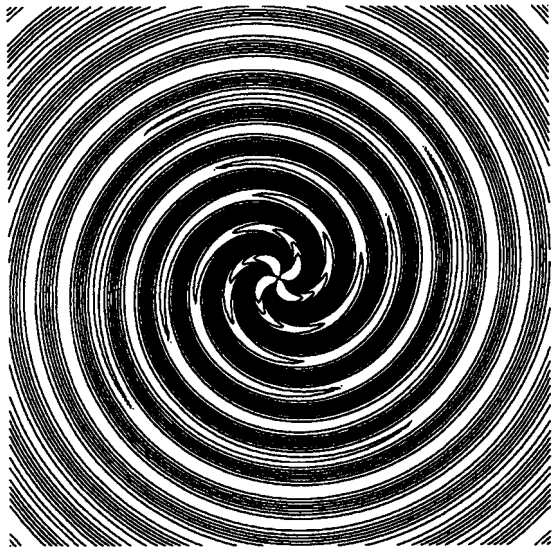

FIGURE 2. Iso-contours of the far-field pressure for a typical solution of (10). Note the double spiral pattern and the nearly cylindrical nature of the waves in the far field.

two-dimensional results, see for instance Ffowcs Williams & Hawkings (1968) and Müller & Obermeier (1967).

3. Flow description

Having summarized relevant acoustic theory and its application to point vortices, we now describe the compressible viscous heat-conducting co-rotating vortices that were simulated numerically. The numerical method will be described below in §3.1.

The vortices are initially separated by distance $2R$ and the swirling flow associated with each vortex (when considered separately) achieves a maximum Mach number, $M_0 = U_0/c_0$, at a radius r_0 from the centre of each vortex core. Figure 1 is a sketch of the flow with definitions of relevant parameters. The initial vorticity distribution for each vortex is Gaussian:

$$\omega = 3.57\frac{U_0}{r_0}\mathrm{e}^{-1.25(r/r_0)^2}, \tag{11}$$

with circulation $\Gamma_0 = 2\pi(0.7)^{-1}U_0 r_0$. The fluid is assumed to be a perfect gas with ratio of specific heats $\gamma = 1.4$ and a Prandtl number of 0.7.

The flow is initially specified as solenoidal and homentropic since it was observed that this choice of initial conditions reduces the magnitude of the initial acoustic transient. For a homentropic solenoidal flow, the following Poisson equation can be solved to find the initial condition for the pressure and density:

$$\left(\frac{P}{\rho}\right)_{,ii} = -\frac{\gamma-1}{\gamma}u_{i,j}u_{j,i}, \tag{12}$$

where it has been assumed that pressure and density are related by $\rho/\rho_0 = (\gamma P/\rho_0 c_0^2)^{1/\gamma}$. Note the similarity of (12) to the typical incompressible Poisson equation for pressure

$$P_{,ii} = -\rho_0 u_{i,j}u_{j,i}.$$

The dynamics of incompressible inviscid co-rotating vortices has received much analytical and computational attention, see for instance Waugh (1992) and Melander,

Zabusky & McWilliams (1988) and references therein. It has been shown that for initially circular vortices with constant vorticity, merger of vortices will take place if $r_0/R > 0.59$ where r_0 is the radius of each vortex. An approximate criterion can be developed for Gaussian vortices by converting each to an equivalent constant-vorticity vortex by equating the first- and second-order moments of vorticity. The equivalent core radius is given by $2r_0/\sqrt{5}$ and the criterion for merger is $r_0/R > 0.67$. Presumably for the case of small viscosity, the inviscid results hold for short times.

We present results in §4 for a case with $M_0 = 0.56$ and $r_0/R = 0.15$ with a Reynolds numbers based on the circulation of each vortex, $Re = \Gamma_0/\nu$, of 7500. The co-rotation Mach number is $M_r = 0.06$, and the period of rotation, τ, based on the initial velocity field is $\tau c_0/R = 105$. This implies that the fundamental wavelength of the sound, λ, which corresponds to $\tau/2$ because of the symmetry, is $\lambda/R = 52.5$. Note the disparity of scales since $\lambda \gg R$. The computational domain extends to two wavelengths in all directions.

The case shows merger after approximately 3 revolutions providing 6 cycles of far field pressure data for the co-rotating vortices followed by data through and after the vortex merger. Based on the criterion given above, merger was not expected. However, viscous effects and/or compressibility may affect whether or not merger takes place. A similar test case, identical in every respect except for the initial condition for density, $\rho(\boldsymbol{x}; t = 0) = \rho_0$, did not merge.

A second, contrasting, simulation was performed for a case that was acoustically non-compact and results are presented in §4.1. The parameters of this second case are $M_0 = 0.56$, $r_0/R = 0.45$, $M_r = 0.18$, Reynolds number based on circulation of $Re = 226 \times 10^3$ and acoustic wavelength of $\lambda/R = 17.5$. The computational domain in this case extended to four wavelengths in all directions. Merger did not occur during the 5 rotations over which the computations were performed. Although the Reynolds number was quite large, no evidence of hydrodynamic instability was observed. Note that since the computations were initially specified free of disturbances, and since the numerical scheme has high spatial and temporal accuracy that minimizes the introduction of numerical disturbances, hydrodynamic instabilities were not expected.

3.1. *Computational considerations*

The two-dimensional unsteady compressible Navier–Stokes equations are solved numerically using a sixth-order compact Padé scheme given by Lele (1992) to evaluate spatial derivatives. The flow is advanced in time with fourth-order Runge–Kutta integration. This combination of spatial and temporal schemes has negligible numerical damping and thus preserves the physical property that, in the absence of viscosity, waves propagate unattenuated. This is essential for the accurate computation of sound waves which have a long spatial and temporal lifetimes and would be noticeably attenuated by numerical dissipation.

An important computational consideration is the disparity of scales between the sound generating region (the vortices) and the sound field. The vortical flow region scales on the separation distance and core diameter whereas the sound field scales on the acoustic wavelength. For the first set of parameters mentioned above, the ratio of these scales, acoustic wavelength to initial half separation distance, is 52.5 to 1. Computations must adequately resolve the near field and still carry the grid out to the far field which is minimally defined as two acoustic wavelengths away from the vortices. A preliminary computation performed on a four-wavelength domain clearly demonstrated that a domain of two acoustic wavelengths was sufficient to reach the far field.

The disparity of scales is handled by the use of a non-uniform mesh which has a small uniform spacing in the near field and a larger uniform spacing in the far field. A region of grid stretching serves as a smooth transition between the near and far fields. Computations of monopole sound sources on both uniform and non-uniform meshes verified that accuracy is not affected by grid stretching provided that the mesh with the largest grid spacing resolves the sound waves. In the computations reported in this paper, the maximum local value of the grid stretching was 5%.

For the first case ($\lambda/R = 52.5$), a square domain of size $-115R$ to $115R$ corresponding to two wavelengths in all directions was used. The grid contained 429^2 mesh points and the near-field spacing was $\Delta x/R = 0.026$ which placed roughly 20 grid points across each vortex core, and the far-field spacing was $\Delta x/R = 2.5$ which allowed 20 grid points per acoustic wavelength. Most of the points were located in the near field. The time step was $\Delta t c_0/R = 0.012$ and the CFL number was initially 0.72.

For the second case ($\lambda/R = 17.5$), a square domain of size $-70R$ to $70R$ corresponding to four wavelengths was used. This computation used a grid containing 453^2 mesh points clustered such that most of the points were in the near field. The near-field spacing was $\Delta x/R = 0.027$ and the far-field spacing was $\Delta x/R = 0.84$. The time step was $\Delta t c_0/R = 0.01$ and the CFL number was initially 0.56.

While it is feasible to construct a non-uniform mesh that resolves the long wavelengths of the expected sound waves, it is not possible to simultaneously resolve the initial acoustic transients. These transients involve sharp spatial gradients that are not resolvable on the far-field mesh. When simulations were first performed using the mesh described above, large-scale reflections of the initial transients occurred as the transients moved through the region of grid stretching. The resulting pressure fluctuations from the spurious reflections were at the same level as the computed sound. This problem was handled by the use of numerical filtering during the initial phases of the computation to remove the short wavelengths associated with the acoustic transient. For this purpose, a fourth-order-accurate compact Padé filter given by Lele (1992) (with the filter parameter, α, chosen as 0.475), which is very effective at removing only the shortest wavelengths, was used, Filtering smooths the transient as it moves through the grid stretching and thus reduces the amount of spurious reflections. The dangers of excessive filtering have been discussed by Mitchell, Lele & Moin (1992).

A major numerical consideration is the choice of boundary conditions. The appropriate boundary conditions for the analysis of flows in free space are non-reflecting boundary conditions which allow waves to freely leave the domain. The zeroth-order boundary conditions described by Colonius, Lele & Moin (1993) were used in these computations. These boundary conditions are based on the work of Giles (1990).

This formulation of the boundary conditions is only exact for one-dimensional waves travelling in, say, the η-direction. In conventional applications of Giles' boundary conditions, the η-direction is taken as the outward normal at the boundary. However, increased accuracy can be obtained by choosing η as the r-direction since the sound waves are nearly cylindrical for this flow. Tests with monopole sources showed that this choice of η significantly reduced reflection errors especially near the corners of the domain. As will be shown below, these boundary conditions proved quite adequate for the present problem.

4. Results and discussion

In this section results of the simulation of co-rotating vortices are presented. A discussion of the near field is presented first followed by a discussion of the far field. Results from a second, contrasting computation that was acoustically non-compact are presented in §4.1.

Figure 3 is a composite picture of the near-field vorticity, clearly showing a time period of co-rotation followed by a merger. After the merger, the resulting elliptical vortex evolves into a single circular vortex. Preceding the merger, the vortices slowly move closer together giving rise to an increased rotation rate in order to conserve angular momentum. The merger itself is quite sudden, occurring in less than 1/2 revolution.

The flow is at all times compressible with the density in the vortex cores initially 54% of ambient, increasing to 90% at the termination of the computations, $tc_0/R = 502$. Similarly, the maximum Mach number in the domain decays rapidly from 0.63 to 0.17. The maximum Mach number is less than 0.3 after the first revolution. Computations of the first-order moments of vorticity show that the flow remains symmetric.

The near-field dilatation is shown in figure 4. Quadrupole structures are evident with axes at 45° to the direction of rotation associated with each vortex. Since it is governed by the wave equation in the far field, the dilatation should decay as $r^{-1/2}$ in the far field. Examination of the quantity $r^{1/2}\nabla\cdot\boldsymbol{u}$ indicated that this far-field behaviour was well developed by 1.2 wavelength from the centre of the flow domain.

According to (6), the connection between the near-field dynamics and far-field sound is the third time derivative of the second-order moments of vorticity. Shown in figure 5 are $\dddot{Q}_1$ and $\dddot{Q}_2$ as defined in (7). The area integrals were computed in a box of size $-4R$ to $4R$ in both the x- and y-directions. The frequency and amplitude of the source terms increase slightly with time as the vortices move closer together. Figure 5 clearly shows a peak in amplitude corresponding to the vortex merger. Note that after merger, the frequency approximately doubles and the amplitude diminishes significantly. The large fluctuations near $tc_0/R = 0$ are the result of transients related to the start of the computation which are amplified due to the third time derivative.

Shown in figure 6 is a contour plot of the far-field pressure at an instant in time when the vortices are still co-rotating; note the similarity to figure 2. There is also evidence of small reflection errors from the boundary.

The temporal evolution of the far-field pressure fluctuations at distances of 1/2 wavelength and 2 wavelengths are shown in figure 7. Note that the nearly sinusoidal nature of fluctuations shows a slight increase in both frequency and amplitude as time moves towards merger; the initial large peak is the acoustic transient. The simulations also show a peak in amplitude at merger. The increase in amplitude can be understood by reference to the results for point vortices developed in §2.2, where the far-field pressure fluctuations were shown to scale as R^{-4}. As the time progresses towards merger, the separation distance, R, decreases giving rise to increased sound levels. The increased pressure fluctuations can also be explained by recognizing that as the vortices approach one another, the rate of rotation must increase to conserve angular momentum. Equation (10) can be manipulated to show that the pressure fluctuations scale as Ω_0^2. The pressure fluctuations shown in figure 7 are 0.01% of the ambient pressure.

Also shown in figure 7 is the prediction of (6) where source terms are the same as shown in figure 5. The integral in (6) was computed using an adaptive quadrature routine; the upper limit of integration was taken as $\cosh^{-1}[c_0(t-t_0)/r]$ where t_0 was

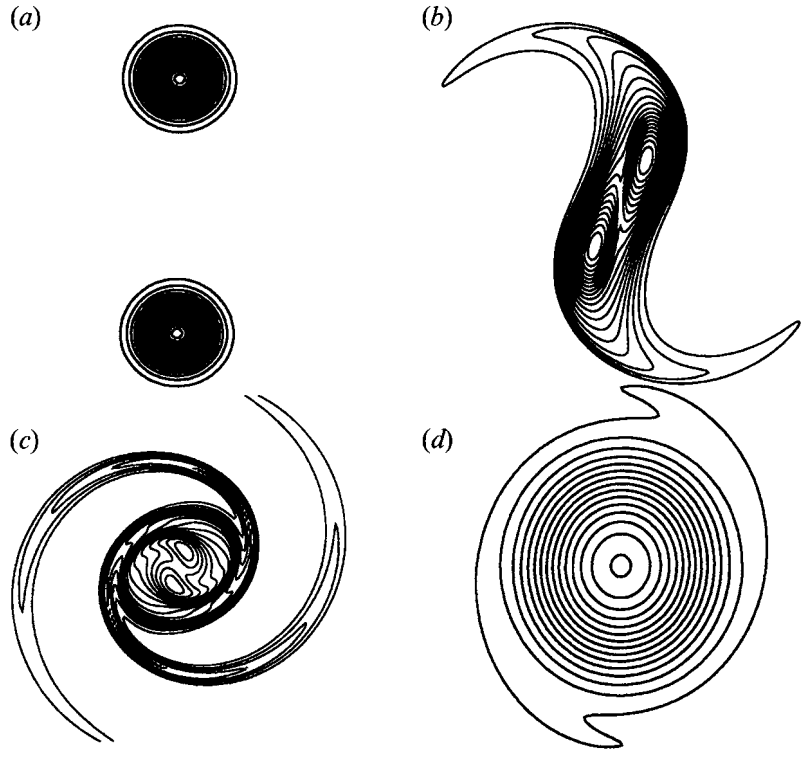

FIGURE 3. Four views of the near-field vorticity showing (*a*) co-rotation ($tc_0/R = 53$), (*b*) merger ($tc_0/R = 343$), (*c*) post-merger vortex ($tc_0/R = 370$), and (*d*) final circular vortex ($tc_0/R = 502$). The contour levels are (*a*) $\omega_{min} = -13.5$, $\Delta\omega = 0.5$; (*b*) $\omega_{min} = -1.0$, $\Delta\omega = 0.05$; (*c*) $\omega_{min} = -0.9$, $\Delta\omega = 0.05$; and (*d*) $\omega_{min} = -0.8$, $\Delta\omega = 0.05$ where the vorticity has been made dimensionless by reference to R and c_0.

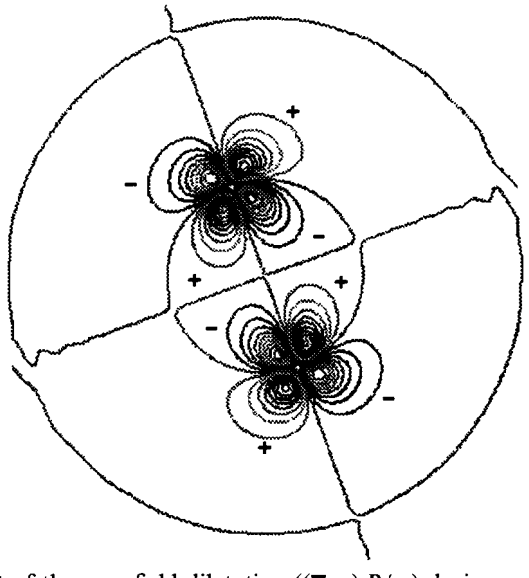

FIGURE 4. Contour plot of the near-field dilatation ($(\nabla \cdot \boldsymbol{u})\, R/c_0$) during co-rotation ($tc_0/R = 239$). The contour levels are centred around zero with increment ± 0.0012.

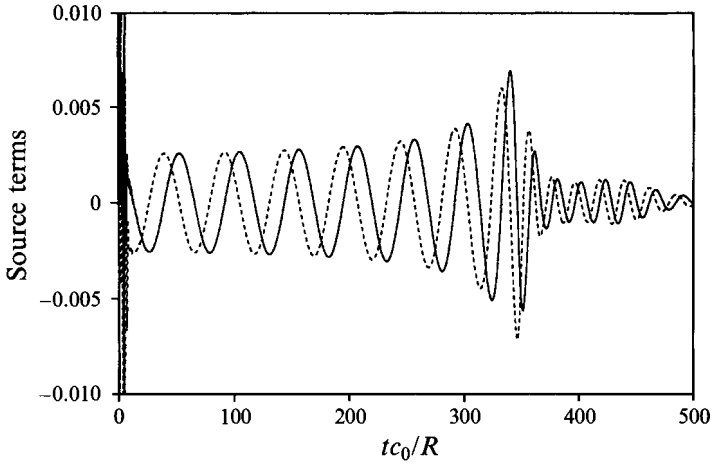

FIGURE 5. Plot of the source terms for Möhring's equation, (6), as defined in (7): ——, $\dddot{Q}_1/(c_0 R)$; and – – –, $Q_2/(c_0 R)$.

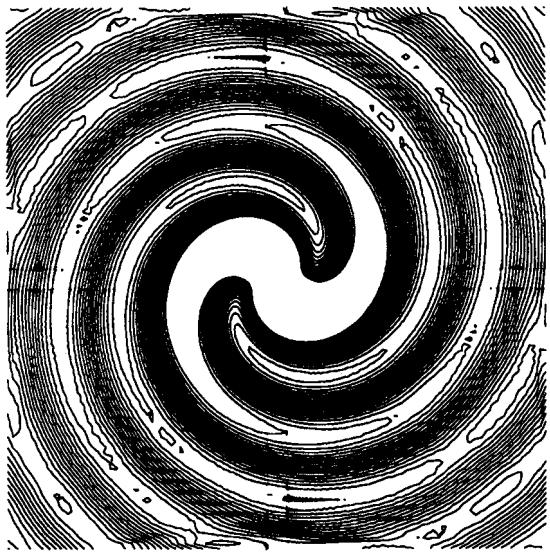

FIGURE 6. The far-field pressure (ambient removed) at $tc_0/R = 185$. The contour levels are from $P/(\rho_0 c_0^2) = \pm 4 \times 10^{-5}$ with $\Delta P/(\rho_0 c_0^2) = 0.05 \times 10^{-5}$. The 'cross' pattern is a plotting illusion caused by the high grid densities near the x- and y- axes.

chosen to be $\tau/4$. This choice of t_0 was sufficient to allow transients associated with the start of the computation to leave the near field. Figure 7 shows excellent agreement between (6) and the results of the direct computation. Agreement is within 3% everywhere even at distances as close as 1/2 wavelength for the amplitude of the pressure fluctuations. Note that the mean pressure in the computation changes after merger. The excellent agreement even at distances as close as 1/2 wavelength was anticipated by the analysis in Appendix B.

These results suggest that Möhring's two-dimensional acoustic analogy can be used with confidence in low-Mach-number two-dimensional compact vortical flows. Kambe & Minota (1983) and Kambe (1986) have compared experiments with vortex rings to predictions of Möhring's three-dimensional result and have also found good agreement.

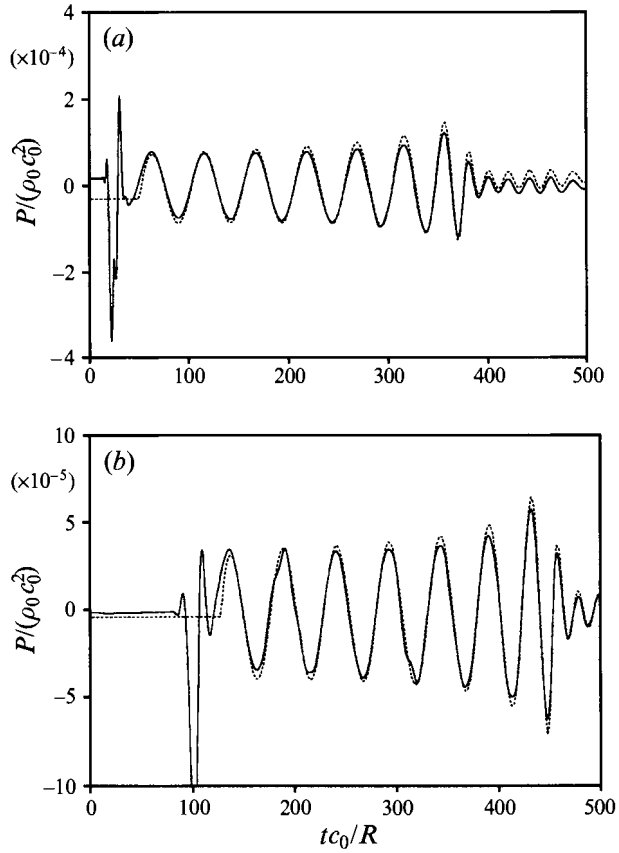

FIGURE 7. Far-field pressure traces at (*a*) $r/\lambda = 1/2$ and (*b*) $r/\lambda = 2$ showing the results of the simulation (——), and the prediction of Möhring's equation (– – –). Both measurement points are located on the positive y-axis.

The far-field sound was also predicted using the acoustic analogy originally due to Powell (1964) where the wave equation was solved numerically with source terms computed using data from the simulation. Equation (3) was solved using sixth-order-accurate central difference for spatial derivatives, fourth-order Runge–Kutta time advancement, and the non-reflecting boundary conditions presented by Engquist & Majda (1979). The computational mesh and time step were the same as those used in the direct simulation of the Navier–Stokes equations. The prediction of the Powell analogy (with the right-hand side of (3) evaluated from the direct numerical simulation) is compared to the results of the simulation in figure 8. The agreement is within 5%. Theoretical derivations typically assume that the density is constant, see for instance Obermeier (1985). However, when the source terms were computed by taking the density at the ambient value, the predicted far-field pressure amplitude was approximately 15% too large.

As was discussed in §2.1, a direct application of Lighthill's analogy in two dimensions suffers from divergent integrals. One approach to avoid this difficulty is to decompose the velocity field into a leading-order component that decays as $1/r$ and a component that decays faster than $1/r$. Thus

$$u_i = \hat{u}_i + \tilde{u}_i, \tag{13}$$

where

$$\tilde{u}_i = 2\Gamma_0 x_i/(2\pi r^2). \tag{14}$$

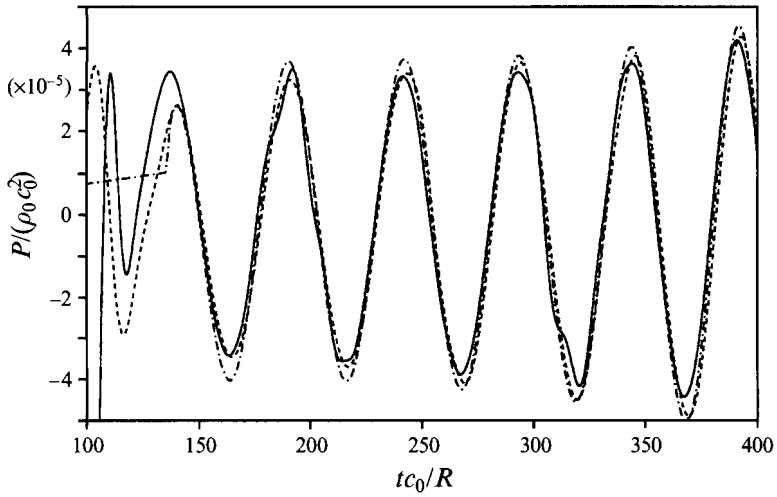

FIGURE 8. Far-field pressure traces at $r/\lambda = 2.0$ showing the results of the simulation (——); the numerical solution of Powell's acoustic analogy (– – –); and the prediction of the modified Lighthill equation (—·—). The measurements point is the same as in figure 7(*b*).

Approximating the Lighthill source term as

$$T_{ij} = \rho u_i u_j$$

and using the decomposition introduced above yields

$$T_{ij} = \rho[\hat{u}_i \hat{u}_j + \hat{u}_i \tilde{u}_j + \tilde{u}_i \hat{u}_j + \tilde{u}_i \tilde{u}_j]. \tag{15}$$

Since solutions of Lighthill's equation depend on the second time derivative of T_{ij}, the last term in (15) can be eliminated because of the time invariance of the circulation and an equivalent source term is

$$\hat{T}_{ij} = \rho[\hat{u}_i \hat{u}_j + \hat{u}_i \tilde{u}_j + \tilde{u}_j \hat{u}_j]. \tag{16}$$

The source terms decay faster than $1/r$, and the far-field pressure is given by (2). It should be noted that in arriving at (16), we have ignored variations in the density (specifically the second time derivative of the density) and thus it is only an approximation to T_{ij}. The results obtained by using the modified terms, as evaluated from the simulation, in the right-hand side of (2) are shown in figure 8. The agreement is quite good. We also attempted to solve Lighthill's equation numerically using the same numerical method used to solve Powell's equation; however, we were unable to recover a meaningful far field. We believe this difficulty is due to the slow algebraic decay rate of both the Lighthill source term and the modified Lighthill source term.

Kambe (1984) and Obermeier (1985) have shown that the presence of viscosity adds a monopole contribution to the far-field sound with amplitude proportional to $\ddot{S}$ where S is the area integral of the entropy. This monopole contribution was computed based on $\ddot{S}$ taken from the simulations and found to be at least two orders of magnitude smaller than the quadrupole contribution. This is in agreement with the scaling suggested by Obermeier (1985).

4.1. *Acoustically non-compact case*

By way of contrast to the excellent agreement between prediction and simulation shown in figure 7, a second simulation was performed for which $M_r = \Gamma_0/(4\pi R c_0) = 0.18$. According to Yates (1978), this case should be acoustically non-compact with pressure fluctuations significantly smaller than the predictions of Möhring's equation.

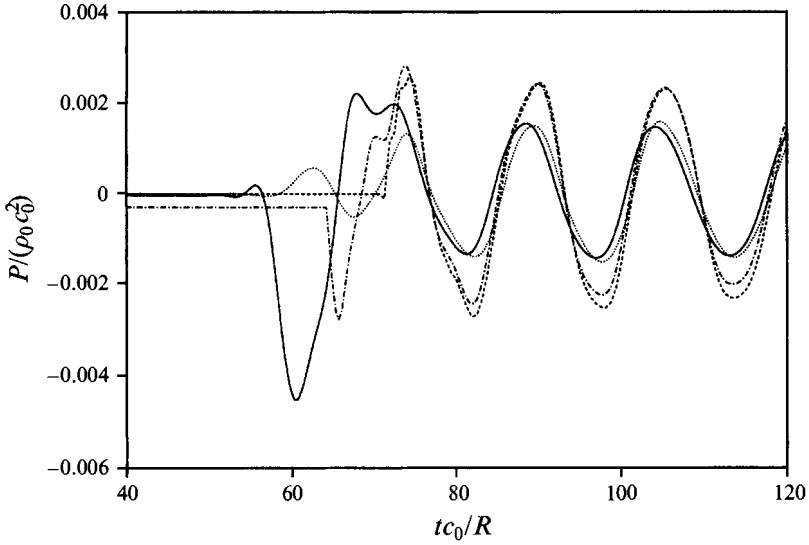

FIGURE 9. Far-field pressure traces at $r/\lambda = 3.6$ for the case of high fluctuating Mach number showing the result of the simulation (——); the prediction of Möhring's equation (– – –); the prediction of Powell's acoustic analogy (·····); and the prediction of the modified Lighthill equation (—·—). The measurement point is located on the positive y-axis.

Figure 9 is a comparison of the pressure fluctuations at 3.6 wavelengths to the prediction of (6). The predicted pressure fluctuations are 65 % too high. The magnitude of the overprediction is in agreement with the analysis of Yates (1978) suggesting that the overprediction is the result of acoustical non-compactness. Although there is a slight phase difference, the frequency of the prediction is the same as the simulation. Also shown in figure 9, are the prediction of Powell's analogy and the prediction of the modified Lighthill equation. The Powell prediction, which makes no assumptions about acoustical compactness, is in good agreement with the simulation whereas the Lighthill's result, which does assume acoustical compactness, is quite similar to the prediction of (6).

There is increased compressibility in the near field for this case with the maximum Mach number decaying from 0.72 to only 0.68 over the duration of the simulation. If we define the fluctuating Mach number as the difference between the maximum Mach number and the co-rotation Mach number, then the fluctuating Mach number is around 0.52. By way of contrast, the fluctuating Mach number for the first case presented is typically around 0.12.

For a different problem which also involves the merging of vortices, the temporal evolution of compressible shear layers, Lele & Ho (1994) found that the decreased acoustic output is a direct effect of the compressibility on the hydrodynamic flow. It was also found that the accuracy of acoustic theory decreased with increased compressibility.

5. Conclusions

Direct computations of the far-field sound from co-rotating compressible vortices have been successfully performed by solution of the Navier–Stokes equations on a grid that includes both near and far fields. In order to perform these computations, the concerns raised by Crighton (1988) had to be successfully addressed.

Results from two cases were presented. In the first case, the vortices undergo a sudden merger after three revolutions. The far-field pressure fluctuations peak at merger and are significantly reduced afterwards. For this case, which was acoustically compact and of low Mach number, the two-dimensional Möhring equation predicted the far-field pressure fluctuations to within 3% even at distances as close as 1/2 wavelength. Predictions based on Powell's analogy and a modified form of Lighthill's analogy were also in good agreement with the simulation. The monopole contribution to the far-field pressure due to viscosity was found to be negligible.

The second case was acoustically non-compact with increased near-field compressibility and the vortices did not merge. For this case, the two-dimensional Möhring equation and the modified Lighthill analogy overpredicted the far-field pressure fluctuations by approximately 65%. This magnitude of the overprediction was in agreement with the analysis of Yates (1978) who considered acoustically non-compact co-rotating point vortices. Powell's analogy, which was solved numerically without assuming acoustical compactness, was able to predict this flow accurately.

Three important conclusions can be drawn about aeroacoustic theory from this work. First, theories based on moments of vorticity (Möhring 1978, 1979) offer a convenient and accurate means to predict far-field sound from compact low-Mach-number flows. Secondly, the direct numerical solution of Powell's equation can be used to determine far-field sound with a minimum of assumptions even if the near field is acoustically non-compact. Thirdly, although a conventional application of Lighthill's equation is not appropriate for compact two-dimensional flows because of divergent integrals, the Lighthill source terms can be modified in certain simple situations to yield accurate predictions.

Although the numerical solution of Powell's equation can be used to determine the far-field sound, the expense of this approach as compared to solving Möhring's equation (or (2)) should be kept in mind. Möhring's equation can be solved in a few seconds of supercomputer time whereas Powell's equation requires a few hours. If the Navier–Stokes equations had only been solved in the near field to obtain source terms, the use of Möhring's equation to predict the far-field sound would have used approximately one fourth of the computational time of the full near- and far-field Navier–Stokes solution. The similar use of Powell's equation would have used approximately 3/4 of the total computation time of the full near- and far-field Navier–Stokes solution. However, even though it is computationally more expensive, the numerical solution of Powell's equation was found to be the only method to accurately predict the acoustically non-compact case discussed in §4.1.

This work was supported by the Office of Naval Research under Grant number ONR-N000014-88-K-0592. Computer time was provided through the Center for Turbulence Research by the NASA Ames Research Center. The authors wish to thank Dr Tim Colonius for many helpful discussions on non-reflecting boundary conditions and for suggesting the velocity decomposition used to modify the Lighthill source terms; and Dr Meng Wang for discussions that led to the approximation of (B 12) by (B 14) and to the form of equation (A 9). Thanks are also due to one of the referees for helpful comments on the original draft of this paper. A preliminary version of some of the results presented here was reported earlier in Mitchell *et al.* (1992).

Appendix A. The solution of Lighthill's equation in two dimensions

Lighthill's equation is

$$\left(\frac{\partial^2}{\partial t^2}-c_0^2\nabla^2_{(y)}\right)\rho=\frac{\partial^2 T_{ij}}{\partial y_i\,\partial y_j}, \tag{A 1}$$

where we have dropped the prime superscript in (A 1) and in what follows. The simplest way to derive the solution in two dimensions is to take the Fourier transform of (A 1) to transform it into a Helmholtz equation:

$$\nabla^2_{(y)}\hat{\rho}+\left(\frac{\Omega}{c_0}\right)^2\hat{\rho}=-\frac{1}{c_0^2}\frac{\partial^2\hat{T}_{ij}}{\partial y_i\,\partial y_j}, \tag{A 2}$$

where $S(t)=\int_{-\infty}^{\infty}\hat{S}(\Omega)\exp(-\mathrm{i}\Omega t)\,\mathrm{d}\Omega$ provided that $\int_{-\infty}^{\infty}S(t)^2\,\mathrm{d}t$ exists. The solution of (A 2) can be found in the usual way by means of the appropriate Green's function,

$$\hat{\rho}(\boldsymbol{x},\Omega)=\frac{\mathrm{i}}{4c_0^2}\int\frac{\partial^2\hat{T}_{ij}(\boldsymbol{y},\Omega)}{\partial y_i\,\partial y_j}\mathrm{H}_0^{(1)}\left(\frac{\Omega\hat{r}}{c_0}\right)\mathrm{d}\boldsymbol{y}, \tag{A 3}$$

where $\hat{r}=|\boldsymbol{x}-\boldsymbol{y}|$ and $\mathrm{H}_0^{(1)}(z)$ is the zeroth-order Hankel function. Using integration by parts and the divergence theorem twice, the spatial derivatives can be brought outside the integral sign:

$$\hat{\rho}(\boldsymbol{x},\Omega)=\frac{\mathrm{i}}{4c_0^2}\frac{\partial^2}{\partial x_i\,\partial x_j}\int\hat{T}_{ij}(\boldsymbol{y},\Omega)\,\mathrm{H}_0^{(1)}\left(\frac{\Omega\hat{r}}{c_0}\right)\mathrm{d}\boldsymbol{y}. \tag{A 4}$$

Furthermore, if $\hat{T}_{ij}$ is acoustically compact, then $\hat{r}$ is well approximated by $r=|\boldsymbol{x}|$ and (A 4) becomes

$$\hat{\rho}(\boldsymbol{x},\Omega)=\frac{\mathrm{i}}{4c_0^2}\frac{\partial^2}{\partial x_i\,\partial x_j}\left(\left[\int\hat{T}_{ij}(\boldsymbol{y},\Omega)\,\mathrm{d}\boldsymbol{y}\right]\mathrm{H}_0^{(1)}\left(\frac{\Omega r}{c_0}\right)\right). \tag{A 5}$$

Performing the spatial derivatives and only retaining the leading-order terms in r, and recognizing that in the far field the pressure and density fluctuations are related via $P=c_0^2\rho$ we obtain

$$\hat{P}(\boldsymbol{x},\Omega)=\frac{\mathrm{i}\Omega^2}{4c_0^2}\frac{x_i x_j}{r^2}\left[\int\hat{T}_{ij}(\boldsymbol{y},\Omega)\,\mathrm{d}\boldsymbol{y}\right]\mathrm{H}_2^{(1)}\left(\frac{\Omega r}{c_0}\right). \tag{A 6}$$

Since we are interested in the far-field solution for P, $\mathrm{H}_2^{(1)}(z)$ will be approximated as $-\mathrm{H}_0^{(1)}(z)$.

The solution in the time domain is found by inverse transforming $\hat{P}$, i.e.

$$P(\boldsymbol{x},t)=\int_{-\infty}^{\infty}\hat{P}(\boldsymbol{x},\Omega)\exp(-\mathrm{i}\Omega t)\,\mathrm{d}\Omega, \tag{A 7}$$

and making use of the integral definition of the Hankel function (Watson 1944, p. 180)

$$\mathrm{H}_0^{(1)}(z)=-\frac{2\mathrm{i}}{\pi}\int_0^{\infty}\mathrm{e}^{\mathrm{i}z\cosh(\xi)}\,\mathrm{d}\xi, \tag{A 8}$$

to arrive at

$$P(\boldsymbol{x},t)=\frac{1}{2\pi c_0^2}\left(\frac{x_i x_j}{r^2}\right)\int_0^{\infty}\frac{\partial^2}{\partial t^{*2}}\left(\int T_{ij}(\boldsymbol{y},t^*)\,\mathrm{d}y^2\right)\mathrm{d}\xi, \tag{A 9}$$

where $t^*=t-r/c_0\cosh(\xi)$.

If the approximation $H_2^{(1)}(z) \approx -H_0^{(1)}(z)$ had not been made, the final result would have been

$$P(\boldsymbol{x}, t) = \frac{1}{2\pi c_0^2}\left(\frac{x_i x_j}{r^2}\right)\int_0^{\infty+\pi i/2} \cosh(2\xi)\frac{\partial^2}{\partial t^{*2}}\left(\int T_{ij}(\boldsymbol{y}, t^*)\,\mathrm{d}y^2\right)\mathrm{d}\xi. \tag{A 10}$$

This form of the result is not as convenient for numerical quadrature because of the exponential growth of $\cosh(2\xi)$.

Appendix B. Development of a two-dimensional vortex sound theory

In this Appendix, we summarize an alternative derivation of Möhring's two-dimensional result using the method of matched asymptotic expansions. This derivation is similar to the derivation given by Kambe (1986) and Kambe *et al.* (1993) of Möhring's three-dimensional result. The basic approach will be to assume that the sound-generating region of the flow is a low-Mach-number compact vortical region for which a series expansion for the velocity potential, valid outside of the vortical region, can be found. By comparing this near-field expansion to the far-field wave solution, the far-field sound will be determined. This procedure depends on the vortical region being acoustically compact in order for there to be a well-defined intermediate region between the vortical region and the acoustic far field. The acoustical compactness condition is equivalent to a low-Mach-number assumption.

The starting point is the two-dimensional Taylor series expansion for the velocity potential given by Kambe (1992, personal communication) (see also Weston & Lu 1982) valid for an incompressible compact flow in the absence of solid boundaries:

$$\Phi = \frac{1}{2\pi}\left[\Gamma\theta + \sum_{n=1}^{\infty}\frac{(-1)^n}{n!}Q_{p_1 p_2 \ldots p_n}\partial_{p_1}\partial_{p_2}\ldots\partial_{p_n}\ln(r)\right], \tag{B 1}$$

where r and θ are the usual polar coordinates with θ measured counter-clockwise from the x-axis and where

$$Q_{p_1 p_2 \ldots p_n} = \int(\boldsymbol{x}\times\boldsymbol{\omega})_{p_1} x_{p_2}\ldots x_{p_n}\,\mathrm{d}\boldsymbol{x}. \tag{B 2}$$

We are assuming that lengths have been made non-dimensional with respect to some characteristic length l associated with the flow in the near field. The near-field pressure implied by (B 1) for large r/l is $-\rho_0\partial\Phi/\partial t$. Since the circulation and Q_i are time invariant for a two-dimensional compact flow (Q_i is a multiple of the linear impulse), the leading-order near-field pressure is given by

$$P = -\frac{\rho_0}{4\pi}\dot{Q}_{ij}\partial_i\partial_j\ln(r). \tag{B 3}$$

In the far field, the pressure is governed by a homogeneous wave equation:

$$\left(\frac{1}{c_0^2}\frac{\partial^2}{\partial t^2} - \nabla^2\right)P = 0.$$

A matched asymptotic expansion is performed to find the far-field pressure due to a harmonic source. The Fourier transform of (B 3) yields a harmonic expression for the near-field pressure:

$$\hat{P} = \frac{\rho_0}{4\pi}(\mathrm{i}\Omega)\,\hat{Q}_{ij}\partial_i\partial_j\ln(r), \tag{B 4}$$

where $S(t) = \int_{-\infty}^{\infty} \hat{S}(\Omega) \exp(-\mathrm{i}\Omega t)\, \mathrm{d}\Omega$. In the far field, the wave equation is transformed into a Helmholtz equation:

$$\nabla^2 \hat{P} + (\Omega/c_0)^2 \hat{P} = 0,$$

which has the general solution (in terms of outgoing waves)

$$\hat{P} = \sum_{n=0}^{\infty} \hat{A}_{p_1 p_2 \ldots p_n} \partial_{p_1} \partial_{p_2} \ldots \partial_{p_n} \mathrm{H}_0^{(1)}\left(\frac{\Omega r}{c_0}\right), \tag{B 5}$$

where $\hat{A}_{p_1 p_2 \ldots p_n}$ is a coefficient tensor to be determined, and where $\mathrm{H}_0^{(1)}(\Omega r/c_0)$ is the zeroth-order Hankel function of the first kind. The asymptotic limit of (B 5) for small $\Omega r/c_0$ is

$$\hat{P} = \frac{2\mathrm{i}}{\pi} \sum_{n=0}^{\infty} \hat{A}_{p_1 p_2 \ldots p_n} \partial_{p_1} \partial_{p_2} \ldots \partial_{p_n} \ln\left(\frac{\Omega r}{c_0}\right). \tag{B 6}$$

Performing the matching between these two regions yields to leading order $\hat{A} = \hat{A}_i = 0$ and

$$\hat{A}_{ij} = \tfrac{1}{8}\rho_0 \Omega \hat{Q}_{ij}. \tag{B 7}$$

Thus to leading order, the sound is predicted to be a quadrupole. The ambiguity in the matching discussed and resolved by Crow (1970) and Kambe *et al.* (1993) does not arise in our approach since the Fourier-transformed equations are being considered. The solution for the far-field pressure is then

$$\hat{P} = \tfrac{1}{8}\rho_0 \Omega \hat{Q}_{ij} \partial_i \partial_j \mathrm{H}_0^{(1)}(\Omega r/c_0).$$

This result can be simplified by evaluating the spatial derivatives and retaining only the leading-order terms in r to yield

$$\hat{P} = \frac{x_i x_j}{r^2} \frac{\rho_0 \Omega^3}{8c_0^2} \hat{Q}_{ij} \mathrm{H}_2^{(1)}\left(\frac{\Omega r}{c_0}\right), \tag{B 8}$$

where the appearance of higher-order Hankel functions is a result of the following relationship for derivatives of the Hankel function (Abramowitz & Stegun 1972, p. 361):

$$\frac{\mathrm{d}}{\mathrm{d}z}\left(\frac{1}{z^n} \mathrm{H}_n^{(1)}(z)\right) = -\frac{1}{z^n} \mathrm{H}_{n+1}^{(1)}(z).$$

It is interesting to note that no terms are neglected in (B 8) since the additional term that results from performing the spatial derivatives is multiplied by $\hat{Q}_{ii} = 0$. So we expect the quadrupole term to be accurate in some intermediate region between the far field and the near field (where r/l is large and $\Omega r/c_0$ is small) and not just in the far field.

The pressure field is obtained by inverse transforming $\hat{P}(\Omega)$ and using the integral definition of the Hankel function (Watson 1944, p. 180),

$$\mathrm{H}_2^{(1)}(z) = \frac{2\mathrm{i}}{\pi} \int_0^{\infty + \pi\mathrm{i}/2} \mathrm{e}^{\mathrm{i}z\cosh(\xi)} \cosh(2\xi)\, \mathrm{d}\xi, \tag{B 9}$$

and can be shown to be

$$P(\boldsymbol{x}, t) = \frac{\rho_0}{4\pi c_0^2} \int_0^{\infty + \pi\mathrm{i}/2} \cosh(2\xi) \left[\frac{x_i x_j}{r^2} \dddot{Q}_{ij}(t^*)\right] \mathrm{d}\xi \tag{B 10}$$

where

$$t^* = t - (r/c_0)\cosh(\xi). \tag{B 11}$$

Since Fourier transforms have been used to express (B 4) and (B 5), (B 10) cannot describe any transient effects associated with initial conditions.

Equation (B 10) can be re-expressed as

$$P(\boldsymbol{x},t)=\frac{\rho_0}{8\pi c_0^2}\int_0^{\infty+\pi\mathrm{i}/2}\cosh(2\xi)\left[\dddot{Q}_1(t^*)\cos(2\theta)+\dddot{Q}_2(t^*)\sin(2\theta)\right]\mathrm{d}\xi, \tag{B 12}$$

where

$$Q_1\equiv 2\iint xy\omega\,\mathrm{d}x\,\mathrm{d}y,\quad Q_2\equiv\iint(y^2-x^2)\,\omega\,\mathrm{d}x\,\mathrm{d}y. \tag{B 13}$$

Equation (B 12) is equivalent to Möhring's two-dimensional result (Möhring 1979). The form of (B 12), also given in Mitchell *et al.* (1992), is not convenient for numerical quadrature because of the exponential growth of $\cosh(2\xi)$. For large z, the approximation $\mathrm{H}_2^{(1)}(z)\approx-\mathrm{H}_0^{(1)}(z)$ may be used in (B 8), modifying (B 12) to

$$P(\boldsymbol{x},t)=\frac{\rho_0}{8\pi c_0^2}\int_0^{\infty}\left[\dddot{Q}_1(t^*)\cos(2\theta)+\dddot{Q}_2(t^*)\sin(2\theta)\right]\mathrm{d}\xi. \tag{B 14}$$

We have used both forms and have found (B 14) to be more robust. The predictions of (B 14) are compared to the directly computed pressure in §4.

Kambe *et al.* (1993) proposed an extension to Möhring's equation that includes higher-order multipoles. While their approach does include terms that are higher order in Mach number than the leading-order quadrupole, it does not appear to be a complete higher order theory in the sense of Crow (1970). However, they show that these higher-order terms are important in the oblique collision of vortex rings. The two-dimensional form of these higher-order multipoles follows directly from the derivation just presented by including more terms in (B 3). The resulting equation is

$$P(\boldsymbol{x},t)=\sum_{n=1}^{N}\left[\frac{\rho_0}{2n!\,c_0^n\,\pi}\right]\left[\frac{x_{p_1}x_{p_2}\cdots x_{p_n}}{r^n}\right]\int_0^{\infty+\pi\mathrm{i}/2}\cosh(n\xi)\,Q^{(n+1)}_{p_1p_2\cdots p_n}(t^*)\,\mathrm{d}\xi, \tag{B 15}$$

where the superscripts on Q_{ij} represent differentiation with respect to t^*.

Appendix C. Multipole expansion of Powell's analogy

In this Appendix, a multipole expansion of Powell's equation is performed that demonstrates how Powell's equation can be used to derive Möhring's equation.

First, we review multipole expansion solution techniques for the wave equation

$$\left(\frac{1}{c_0^2}\frac{\partial^2}{\partial t^2}-\nabla^2\right)P=g(\boldsymbol{x},t).$$

In three dimensions, the multipole solution of the wave equation is (see Goldstein 1976)

$$P=\left(\frac{1}{4\pi}\right)\left(\frac{1}{r}\right)\left[\mathrm{A}\left(t-\frac{r}{c}\right)+\frac{x_i}{c_0 r}\dot{B}_i\left(t-\frac{r}{c}\right)+\frac{x_ix_j}{c_0^2r^2}\ddot{\mathrm{C}}_{ij}\left(t-\frac{r}{c}\right)+\ldots\right],$$

where

$$\mathrm{A}(t)=\int g(\boldsymbol{x},t)\,\mathrm{d}\boldsymbol{x},\quad \mathrm{B}_i(t)=\int x_i\,g(\boldsymbol{x},t)\,\mathrm{d}\boldsymbol{x},\quad \mathrm{C}_{ij}(t)=\frac{1}{2}\int x_ix_j\,g(\boldsymbol{x},t)\,\mathrm{d}\boldsymbol{x}.$$

The result in two dimensions is quite similar and can be found using the same method given in Goldstein:

$$P = \frac{1}{2\pi}\int_0^{\infty+\pi i/2}\left[\mathrm{A}\left(t-\frac{r}{c}\cosh(\xi)\right)+\frac{x_i}{c_0 r}\cosh(\xi)\,\dot{\mathrm{B}}_i\left(t-\frac{r}{c}\cosh(\xi)\right)\right.$$
$$\left.+\frac{x_i x_j}{c_0^2 r^2}\cosh(2\xi)\,\ddot{\mathrm{C}}_{ij}\left(t-\frac{r}{c}\cosh(\xi)\right)+\ldots\right]\mathrm{d}\xi,$$

with A, B_i, C_{ij} as defined above. The above solutions assume that the sources are acoustically compact and that the wave equation is being solved in free space.

We now use the general multipole solution to manipulate an extended version of Powell's equation in order to explicitly determine the monopole, dipole and quadrupole contributions to the far-field sound. We shall use a version of Powell's analogy extended to allow a force, $\boldsymbol{f}$, applied to the source region

$$\left(\frac{1}{c_0^2}\frac{\partial^2}{\partial t^2}-\nabla^2\right)P = \rho_0\,\boldsymbol{\nabla}\cdot\left(\boldsymbol{\omega}\times\boldsymbol{u}+\boldsymbol{\nabla}\frac{u^2}{2}-\boldsymbol{f}\right),$$

where a low-Mach-number assumption has been used to set the density equal to ρ_0. In what follows, we also assume that there is a compact flow and a compact source.

The monopole term, A, can be shown to be zero using the divergence theorem. The dipole term after integration by parts and use of the divergence theorem becomes

$$\mathrm{B}_i = -\rho_0\int\left(\boldsymbol{\omega}\times\boldsymbol{u}+\boldsymbol{\nabla}\frac{u^2}{2}-\boldsymbol{f}\right)_i\mathrm{d}\boldsymbol{x}.$$

Using the inviscid Euler equations yields

$$\mathrm{B}_i = \partial\mathscr{P}_i/\partial t,$$

where $\mathscr{P}_i$ is the linear impulse. In a similar manner, the quadrupole term can be shown to be

$$\mathrm{C}_{ij} = \partial\mathscr{Q}_{ij}/\partial t,$$

where the angular impulse is related to the tensor $\mathscr{Q}_{ij}$, i.e. the angular impulse is given by $\epsilon_{ijk}\,\mathscr{Q}_{jk}$.

The net source terms implied by this multipole expansion are

$$\left(\frac{1}{c_0^2}\frac{\partial^2}{\partial t^2}-\nabla^2\right)P = -\frac{\partial}{\partial x_i}(\dot{\mathscr{P}}_i(t)\,\delta(\boldsymbol{x}))+\frac{\partial^2}{\partial x_i\,\partial x_j}(\dot{\mathscr{Q}}_{ij}(t)\,\delta(\boldsymbol{x}))+\ldots, \tag{C 1}$$

which is valid in both two and three dimensions. The difference in the two cases is given by differences in the free-space Green's function and the expressions for $\mathscr{P}_i$ and $\mathscr{Q}_{ij}$. In three dimensions, $\mathscr{P}_i$ and $\mathscr{Q}_{ij}$ are given as (Cantwell 1986, Batchelor 1967):

$$\mathscr{P}_i^{(3d)} = \frac{\rho_0}{2}\int[\boldsymbol{x}\times\boldsymbol{\omega}]_i\,\mathrm{d}x^3, \quad \mathscr{Q}_{ij}^{(3d)} = \frac{\rho_0}{3}\int x_i[\boldsymbol{x}\times\boldsymbol{\omega}]_j\,\mathrm{d}x^3, \tag{C 2}$$

and in two dimensions:

$$\mathscr{P}_i^{(2d)} = \rho_0\int[\boldsymbol{x}\times\boldsymbol{\omega}]_i\,\mathrm{d}x^2, \quad \mathscr{Q}_{ij}^{(2d)} = \frac{\rho_0}{2}\int x_i[\boldsymbol{x}\times\boldsymbol{\omega}]_j\,\mathrm{d}x^2. \tag{C 3}$$

This form of the acoustic analogy shows that sound is generated by fluctuations in

$\mathscr{P}_i$ and $\mathscr{Q}_{ij}$. Since $\mathscr{P}_i$ and $\mathscr{Q}_{ij}$ are proportional to moments of the vorticity field, it is clear that certain types of vortex motion give rise to sound radiation. In the absence of applied forces and solid boundaries, the linear impulse is an invariant of the flow and no dipole sound is expected.

These solutions of Powell's analogy are identical to Möhring's solutions in both two and three dimensions.

REFERENCES

ABRAMOWITZ, M. & STEGUN, I. 1972 *Handbook of Mathematical Functions*. Dover.

BATCHELOR, G. K. 1967 *An Introduction to Fluid Dynamics*. Cambridge University Press.

CANTWELL, B. 1986 Viscous starting jets. *J. Fluid Mech.* **173**, 159–189.

COLONIUS, T., LELE, S. K. & MOIN, P. 1991 Scattering of sound waves by a compressible vortex. *AIAA Paper* 91–0494.

COLONIUS, T., LELE, S. K. & MOIN, P. 1993 Boundary conditions for direct computation of aerodynamic sound generation. *AIAA J.* **31**, 1574–1582.

COLONIUS, T., LELE, S. K. & MOIN, P. 1994 The scattering of sound waves by a vortex – numerical simulations and analytical solutions. *J. Fluid Mech.* **260**, 271–298.

CRIGHTON, D. G. 1988 Goals for computational aeroacoustics. In *Computational Acoustics: Algorithms and Applications* (ed. J. C. Hardin & M. Y. Hussaini). Elsevier.

CROW, S. C. 1970 Aerodynamic sound emission as a singular perturbation problem. *Stud. Appl. Math.* **49**, 21–44.

ENGQUIST, B. & MAJDA, A. 1979 Radiation boundary conditions for acoustic and elastic wave calculations. *Commun. Pure Applied Math.* **23**, 313–357.

FFOWCS WILLIAMS, J. E. & HAWKINGS, D. L. 1968 Shallow water wave generation by unsteady flow. *J. Fluid Mech.* **31**, 779–788.

GILES, M. B. 1990 Nonreflecting boundary conditions for Euler equation calculations. *AIAA J.* **12**, 2050–2058.

GOLDSTEIN, M. E. 1976 *Aeroacoustics*. McGraw Hill.

HOWE, M. S. 1975 Contributions to the theory of aerodynamic sound, with application to excess jet noise and the theory of the flute. *J. Fluid Mech.* **71**, 625–673.

KAMBE, T. 1984 Influence of viscosity on aerodynamic sound emission in free space. *J. Sound Vib.* **95**, 351–360.

KAMBE, T. 1986 Acoustic emissions by vortex motions. *J. Fluid Mech.* **173**, 643–666.

KAMBE, T. & MINOTA, T. 1983 Acoustic wave radiated by head-on collisions of two vortex rings. *Proc. R. Soc. Lond.* A **386**, 277–308.

KAMBE, T., MINOTA, T. & TAKAOKA, M. 1993 Oblique collision of two vortex rings and its acoustic emission. *Phys. Rev.* E **48**, 1866–1881.

LAMB, H. 1932 *Hydrodynamics*. Dover.

LELE, S. K. 1992 Compact finite difference schemes with spectral-like resolution. *J. Comput. Phys.* **103**, 16–42.

LELE, S. K. & HO, C. M. 1994 Acoustic radiation from temporally evolving free shear layers. *Internal Report, Stanford University*.

LIGHTHILL, M. J. 1952 On sound generated aerodynamically I. General theory. *Proc. R. Soc. Lond.* A **211**, 564–587.

LYAMSHEV, L. M. & SKVORTSOV, A. T. 1988 Sound radiation by localized vortices in a slightly compressible medium (Review). *Sov. Phys. Acoust.* **34**, 447–59.

MELANDER, M. V., ZABUSKY, N. J. & MCWILLIAMS, J. C. 1988 Symmetric vortex merger in two dimensions: causes and conditions. *J. Fluid Mech.* **195**, 303–340.

MITCHELL, B. E., LELE, S. K. & MOIN, P. 1992 Direct computation of the sound from a compressible co-rotating vortex pair. *AIAA Paper* 92–0374.

MÖHRING, W. 1978 On vortex sound at low Mach number. *J. Fluid Mech.* **85**, 685–691.

MÖHRING, W. 1979 Modelling low Mach number noise. In *Mechanics of Sound Generation in Flows* (ed. E.-A. Müller), pp. 85–96. Springer.

MÜLLER, E. A. & OBERMEIER, F. 1967 The spinning vortices as a source of sound. In *Proc. Conf. on Fluid Dynamics of Rotor and Fan Supported Aircraft at Subsonic Speeds*. AGARD.

OBERMEIER, F. 1985 Aerodynamic sound generation caused by viscous processes. *J. Sound Vib.* **99**, 111–120.

POWELL, A. 1964 Theory of vortex sound. *J. Acoust. Soc. Am.* **36**, 177–195.

WATSON, G. N. 1944 *A Treatise on the Theory of Bessel Functions*. Cambridge University Press.

WAUGH, D. 1992 The efficiency of symmetric vortex merger. *Phys. Fluids* A **4**, 1745–1758.

WESTON, R. P. & LU, C. H. 1982 Approximate boundary condition procedure for the two-dimensional numerical solution of vortex wakes. *AIAA Paper* 82–0951.

YATES, J. E. 1978 Application of the Bernoulli enthalpy concept to the study of vortex noise and jet impingement noise. *NASA Contractor Rep.* 2987.